Annals of Nuclear Energy 99 (2017) 399–409

Contents lists available at ScienceDirect

Annals of Nuclear Energy

journal homepage: www.elsevier.com/locate/anucene

The experimental determination of the $^{238}U(n,\gamma)$ and total fission reaction rates along the pellet radius of the IPEN/MB-01 reactor

Luís Felipe Liambos Mura, Adimir dos Santos *, Douglas Borges Domingos, Pedro Carlos Russo Rossi, Rogério Jerez

Instituto de Pesquisas Energéticas e Nucleares, Av. Lineu Prestes 2242, CEP: 05508-000 São Paulo, SP, Brazil

ARTICLE INFO

Article history:
Received 29 June 2016
Received in revised form 23 September 2016
Accepted 27 September 2016
Available online 20 October 2016

Keywords:
Spectral indices
IPEN/MB-01 reactor
^{238}U and ^{235}U reaction rates
Intra-pellet measurements

ABSTRACT

This work presents a new experimental approach to determine experimentally the reaction rate along the pellet radius of a research reactor facility. The methodology employs concentric hollow cylindrical lead collimators together with gamma-ray spectrometry in a special kind of HPGe detector for the discrimination of very low gamma energy emitted by ^{239}Np and ^{99}Mo. The ^{238}U neutron capture and total fission rates were inferred, respectively, from the 106.2 keV gamma emitted by ^{239}Np and from the 140.51 keV gamma-ray emitted by ^{99}Mo. These lower gamma-ray energies allow the thickness of the lead collimator to be small enough so that the correction factors applied to the procedure were minimized. This kind somewhat challenging experiment was successfully performed at the IPEN/MB-01 research reactor facility. The experiments are claimed to be well-defined, and they are suitable for a benchmark. The measured values of the total fission rates are mainly due to the thermal fissions in ^{235}U since in the IPEN/MB-01 reactor nearly 85% of the total fissions occur in the thermal neutron energy region. The theoretical analyses were performed using MCNP-5 together with the ENDF/B-VII.0 library. The analyses reveal a very good agreement between the calculated and experimental results for the ^{238}U epithermal neutron capture reaction rates. However, the same can not be said for the thermal reaction rates which show discrepancies both in magnitude as well as in the shape of the attenuation of the reaction rates inside of the fuel pellet. The suspected reason for these discrepancies is the shape of the ^{235}U cross sections below 0.3 eV which might be different from that adopted in the ENDF/B-VII.0 library.

1. Introduction

In the fuel burnup evaluation process it is crucial to take into account the radial distribution of power and temperature inside the fuel pellet. This is usually achieved by dividing the fuel pellet into concentric cylinders to treat flux non-uniformity such as the resonance Doppler broadening in the actinide nuclides when temperature increases (Goltsev et al., 2003). In this context, the reactor codes that deal with such phenomena are very important tools because they make possible the calculations of neutron flux, criticality and burnup distribution in the nuclear fuel. These codes generally use stochastic methods such as Monte Carlo (Eckhardt, 1987) and deterministic methods like SDDM (Spatially Dependent Dancoff Method) (Matsumoto et al., 2005). In both cases it is necessary to validate the calculation methodology and their related nuclear data libraries by comparison with appropriate experimental data. The basic premise is how to apply microscopic cross sections in macroscopic systems of the reactor without losing the characteristics of the physical reality of the analyzed system.

Because of its importance in calculations, many of the existing nuclear data and a significant portion of all cross section processing codes are dedicated to treatment of the behavior of the actinide resonance self and mutual shielding (De Kruijf, 1993), especially in deterministic codes where homogenization of the materials present in the reactor core and reflector and multigroup treatment for the neutron energy domain are of major concern.

There has been a great interest in distribution measurements of nuclear reaction rates inside of the fuel rods and pellets (Andrianov et al., 2008; Matzke, 1992). This interest arose from the need to effectively understand the behavior of the resonance self and mutual shielding of the actinide nuclides such as ^{235}U, ^{238}U, ^{239}Pu and ^{240}Pu in the fuel pellets (Stoker and Weiss, 1996; Hwang and Wigner, 2004). Such measurements are used to homogenize the nuclear fuel burnup rate that varies along the radial direction of the fuel pellets optimizing core calculations.

* Corresponding author at: Instituto de Pesquisas Energéticas e Nucleares – IPEN/CNEN-SP, Centro de Engenharia Nuclear (CEN), Av. Prof. Lineu Prestes, 2242, 05508-000 – Cidade Universitária, São Paulo, SP, Brazil.

E-mail addresses: asantos@ipen.br (A. dos Santos), rjerez@ipen.br (R. Jerez).

http://dx.doi.org/10.1016/j.anucene.2016.09.046
0306-4549/

For several years, the mathematical methods and nuclear data libraries applied to the reactor physics have imposed severe restrictions on the calculated predictions. It was common to adopt empirical procedures such as cross sections adjustment to obtain better agreement between theory and experiment (Hellstrand, 1996). The main progresses in the comparison between theory and experiment are due to advances in the following points: improvement of nuclear data, new techniques of nuclear parameter measurements and a significant increase in computer processing speed. Nowadays, mathematical and numerical methods have matured to such a stage of development that it is believed that the major source of the uncertainty in the reactor physics codes reside in their basic nuclear data. Consequently, a major problem in the verification and validation of existing models to treat non-uniformity of nuclear transmutation is the lack of suitable experiments that provide possible physical quantities to be treated by these mathematical models. In this context the IPEN/MB-01 research reactor facility is extremely important. This facility consists of a 28×26 rectangular array of UO_2 fuel rods 4.3486 wt% enriched uranium as UO_2 and clad by stainless steel (SS-304) inside a light water tank. The maximum allowed power is 100 W. The control of the IPEN/MB-01 reactor is via two control banks diagonally placed. The square pitch of the IPEN/MB-01 reactor was chosen to be close to the optimum fuel-to-moderator ratio (maximum k_∞). This feature favors the thermal neutron energy region and mainly the ^{235}U fission events. This facility has well defined geometric and material data composition and many of its experiments have been accepted as international benchmarks in several critical configuration experiments (dos Santos et al., 2004) and in several other classical reactor physics experiments (dos Santos et al., 2005).

The distribution measurements of nuclear reaction rates along the radial direction of the fuel pellets are commonly performed using powerful techniques such as EPMA (electron probe microanalysis) and SIMS (secondary ion mass spectrometry). The spatial distribution of uranium, plutonium and certain fission products can be analyzed quantitatively through them. Both techniques have detection limits of approximately 10^{13} atoms per cubic centimeter. However, in the case of IPEN/MB-01 the fission rate is approximately 10^8 reactions/(cm^3-sec), so these techniques are not able to measure quantitatively the distribution of the secondary nuclear reaction products in the reactor due to its very low concentration.

In recent works carried out by Macku et al. (2006, 2007), direct and indirect measurements of nuclear reaction rates were carried out along the radial direction of fuel pellets using the SVEA-96 reactor Optima2, a BWR critical unit type in the PROTEUS complex (Williams et al., 1998). In the first work, direct measurements of capture reaction rate were made in the ^{238}U foils (C8) and fission measurements in ^{235}U foils (F5) that had been irradiated between the fuel rod pellets. After irradiation the foils were "cut" into rings and measured separately enabling sampling of four different radial regions of the fuel. The results of these measurements were compared to those calculated by MCNP-4C (Briesmeister, 2000) code and Casmo-4 code (Edenius et al., 1995). This type of measurement induced high uncertainty because part of the irradiated material is lost during the cutting process. In the second study, copper foils were used within the fuel rods for determining the spatial distribution of $^{63}CU(n,\gamma)^{64}Cu$ reaction. This reaction is of interest because the 1/v cross-section region of this reaction is similar to the ^{235}U fission reaction. The results were compared to those calculated with the MCNP-4C code. Although the shape of the cross section of $^{63}CU(n,\gamma)$ and $^{235}U(n,f)$ is similar below 0.3 eV, the radial fission profile was not fully determined.

The objective of this work is to present a new sampling technique based on the utilization of Pb collimators, making it possible to measure the radiative neutron capture in ^{238}U and the total fission rates in six different radial regions of an irradiated thin UO_2 disk employing the IPEN/MB-01 research reactor facility. The main advantage of this technique over the previous methods already presented is the maintenance of the integrity of irradiated disks during and after the measurements allowing the measurement to be repeated to verify its reproducibility. There is a great scarcity of experimental data of nuclear reaction rate distributions inside of the fuel pellets. This work aims to contribute to providing high quality experimental data, helping to address this deficiency and collaborating directly for code and related nuclear data library validations in the reactor physics area.

2. Experimental methodology and procedure

The nuclear reaction rates along the radius of the fuel pellets are obtained using the activation analysis technique employing a very thin UO_2 disk (about 0.9 mm thickness and 4.3% enrichment obtained from the UO_2 pellets of the facility). The gamma spectrometry of this disk is performed by the Gamma Detection System (GDS) which is composed of a very thin set of Pb collimators and a special HPGe (High Pure Germanium) detector. The Pb collimators are cylindrical and have concentric holes with variable diameters at their center. Because of its high sensitivity, activation analysis has been used in many IPEN/MB-01 experiments. The thermal flux in this facility is about 10^8 (n/cm^2 s) which is appropriate for many activation analysis experiments. This low neutron flux induces low radioactive levels in the irradiated targets, enabling their handling and reducing saturation effects in HPGe detectors.

The measurements of the radiative capture rate in ^{238}U and fission rates in both ^{238}U and ^{235}U require that the UO_2 disk be inserted between the fuel pellets of the fuel rod. An experimental demountable fuel rod, similar to the one used in the reactor was employed to cope with this task. Tests were conducted to demonstrate the UO_2 radial mass homogeneity in this fuel disk by measuring its thickness in several positions. That was a way to infer the mass homogeneity in the UO_2 disk. This UO_2 disk is inserted between the tenth and eleventh pellets of the rod; i.e. nearly 105.5 mm from the bottom of the active region of the core. This position is in the asymptotic region of the core and far enough from the control banks so that undesirable flux perturbation is prevented. The experimental fuel rod is irradiated at the central position of the core (position M-14 in Fig. 1) for 1 h at 100 W power level (maximum power of the IPEN/MB-01 reactor).

The core configuration in this experiment consists of an array of 28×26 with 680 fuel rods with 24 Ag–In–Cd control rods, which control the reactivity, and 24 B_4C safety rods kept at a position 19.20 cm above the active region of the core during the experiment. Fig. 1 shows the radial configuration in the experiments. A complete description of the IPEN/MB-01 reactor may be found in (Briggs, 2012).

Two irradiations, respectively, with and without cadmium sleeves are performed. In the first irradiation, a cadmium sleeve was wrapped around the experimental fuel rod at the disk position to discriminate thermal and epithermal neutrons from the second irradiation; i.e., the bare irradiation. The cadmium sleeve is 7.0 cm long and 0.5 mm thick and is inserted in the reactor core using the apparatus shown in Fig. 2. This apparatus has a Lucite ruler that is used to hold the cadmium sleeve. The height of the ruler can be adjusted relatively to the bottom of the fuel rod.

After irradiation, the UO_2 disk is taken to the Gamma Detection System (GDS), which performs the gamma spectrometry of the nuclear reaction products arising from the reaction rates occurring in ^{238}U and in ^{235}U. The UO_2 disk is covered with the Pb collimator so that the GDS system measures mainly the gammas emitted by

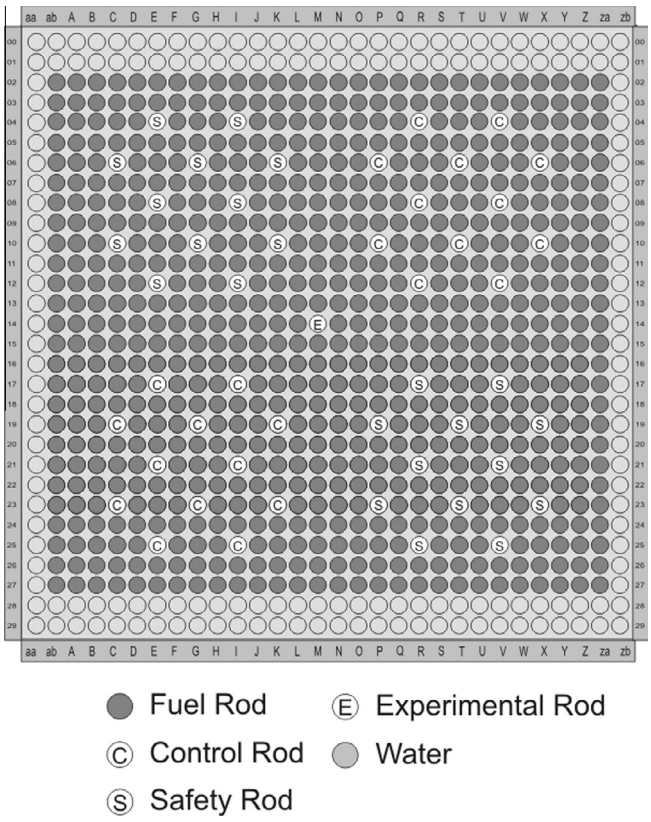

Fig. 1. IPEN/MB-01 core configuration for the reaction rate experiments.

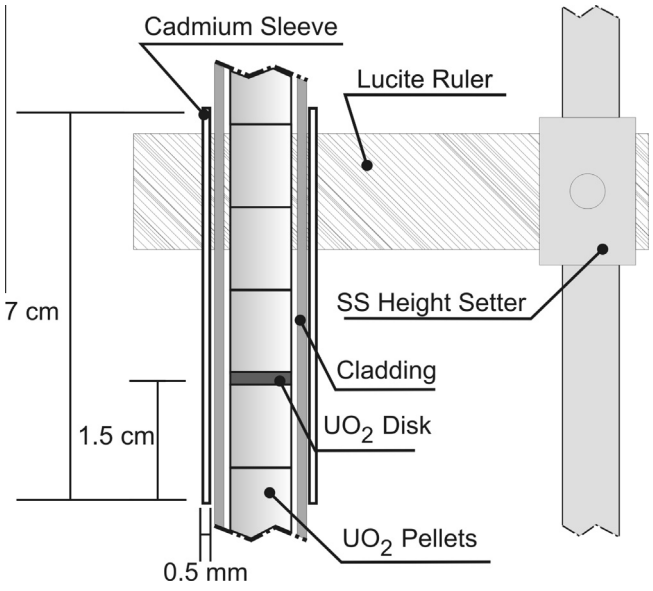

Fig. 2. Cadmium support mechanism.

the uncovered regions of the fuel disk. The UO_2 disk, the collimator and the HPGe detector are aligned in a symmetric way as shown in Fig. 3. The effectiveness of the Pb collimator as well as the detector dead time is improved if the GDS system measures preferentially gammas with as low an energy as possible. This was accomplished by employing a special Canberra HPGe GL type detector with high resolution and relatively high detection efficiency for the low energy gammas (50–200 keV) of the nuclear reaction products chosen for the experiments.

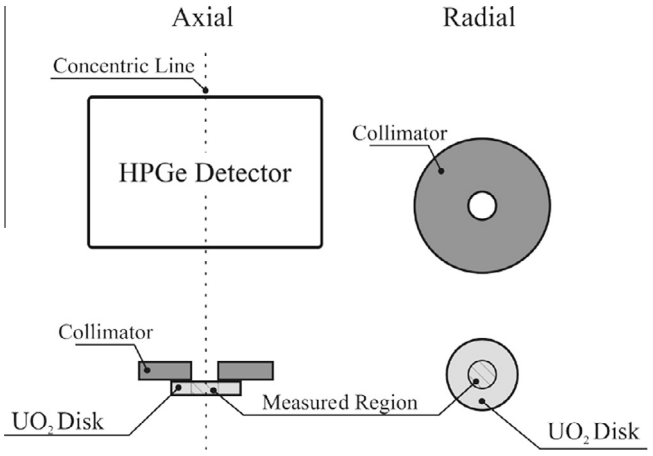

Fig. 3. The GDS system.

After an exhaustive analysis for the selection of the gamma energies and emitters, the following measurement scheme was found to fulfill the objectives of this work. The radiative capture reaction rate in ^{238}U will be determined by measuring the count rate of gammas with 106.2 keV which are the lowest detectable energy decay gammas from ^{239}Np (half-life of 2.335 days). This gamma has 27.2% emission probability allowing high counting rates. The ^{239}Np is the product of the decay of ^{239}U (product of neutron capture in ^{238}U). The total fission reaction rate in uranium will be determined by measuring the activity of ^{99}Mo. This fission product has high fission yield and it emits gammas with 140.51 keV which are the lowest detectable energy decay gammas from the fission products with high counting rate during the gamma spectrometry. The ^{99}Mo decay scheme is shown in Fig 4. To determinate the activity of ^{99}Mo (at the end of irradiation), it is necessary to consider both decay pathways that result in the emission of the 140.51 keV gamma. ^{99}Mo decays directly to ^{99}Tc and decays in a second pathway to ^{99m}Tc with a half-life of 6 h and a branching of 86.5%. Subsequently ^{99m}Tc decays to ^{99}Tc emitting the gamma 140.51 keV.

The choice of these gamma emitters and corresponding energies mentioned previously allowed the Pb collimator height to be small (1.5 mm) which is very appropriate for the experiment quality and purposes. Moreover, it avoided major correction factors due to the Pb collimator presence in the GDS system. The whole GDS system is covered with Pb shielding to avoid undesirable background in the detector.

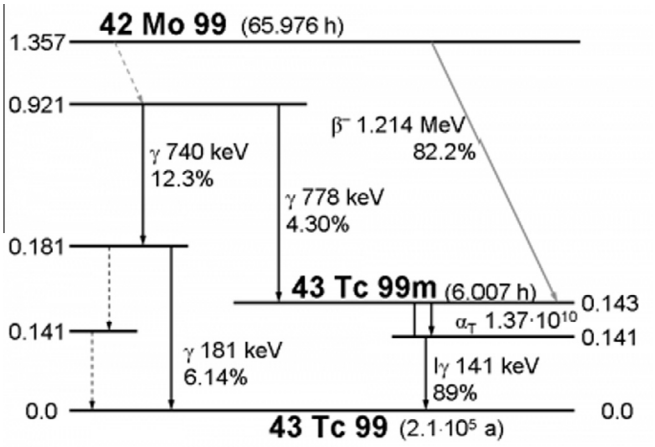

Fig. 4. The ^{99}Mo decay chain.

The Canberra HPGe GL detector efficiency curve was determined using standard ^{152}Eu and ^{133}Ba sources having the same geometry as the UO_2 disk. Polynomial interpolation defined by Gray (Gray and Ahmad, 1985) was adopted to determine the efficiencies at the desired energies (106.2 and 140.5 keV) with associated uncertainties of around 4.2%.

^{99}Mo has been utilized to infer the fission rates in several other works (Sanchez et al., 2014 and Charlton et al., 1996).

2.1. ^{238}U radiative capture rate determination

The absolute values of radiative capture rate in ^{238}U are obtained from the following relationship proposed by Nakajima and Akai (1994, 1995) and Nakajima et al. (1994):

$$C8 = \frac{\lambda^{U9} - \lambda^{Np}}{\lambda^{U9}} \frac{C_0 \cdot \lambda^{Np} \cdot f_{abs}^{Np} \cdot F_{rp}}{I^{Np} \cdot \varepsilon^{Np} \cdot [1 - e^{(-\lambda^{Np} \cdot ti)}] \cdot [1 - e^{(-\lambda^{Np} \cdot tc)}]}, \quad (1)$$

where C_0 is the106.2 keV photopeak intensity (countings) of ^{239}Np at the end of the irradiation, f_{abs}^{Np} is the self-shielding factor of the fuel disk for gammas of 106.2 keV, I^{Np} is the gamma emission probability at 106.2 keV from ^{239}Np decay, ε^{Np} is the detector efficiency for gammas of 106.2 keV, λ^{Np} is the ^{239}Np decay constant, λ^{U9} is the ^{239}U decay constant, t_i is the irradiation period, t_c counting interval and F_{rp} is the ramp factor (correction due to the reactor power rise from 0 to 100 W).

The ^{99}Mo activity at the end of irradiation is obtained considering simultaneously the contribution of the gammas of 140.51 keV arising from the decays of both ^{99}Mo and ^{99m}Tc as shown in the decay scheme of Fig. 4. The final result is given in Eq. (2):

$$A_{Mo}^0 = \frac{\frac{Net}{\varepsilon} - A}{D(B - C) + E}, \quad (2)$$

where A_{Mo}^0 is the ^{99}Mo activity at the end of the irradiation, and the constants A through E are defined as:

$$A = \frac{\gamma_{Tc} I_{Tc} A_{Tc}^0}{\lambda^{Tc}} e^{-\lambda^{Tc} t_e} (1 - e^{-\lambda^{Tc} \Delta t})$$

$$B = \frac{e^{-\lambda^{Mo} t_e}}{\lambda^{Mo}} (1 - e^{-\lambda^{Mo} \Delta t})$$

$$C = \frac{e^{-\lambda^{Tc} t_e}}{\lambda^{Tc}} (1 - e^{-\lambda^{Tc} \Delta t})$$

$$D = \frac{\gamma_{Tc} I_{Tc} \lambda^{Tc}}{\lambda^{Tc} - \lambda^{Mo}}$$

$$E = \frac{\gamma_{Mo} I_{Mo}}{\lambda^{Mo}} e^{-\lambda^{Mo} t_e} (1 - e^{-\lambda^{Mo} \Delta t}),$$

where *Net* is the counts detected by the GDS, ε is the detection efficiency, A_{Tc}^0 is the activity of ^{99m}Tc at the end of irradiation, γ_{Tc} is the branch of ^{99m}Tc decay path, I_{tc} is the emission probability of 140.51 keV gamma of the ^{99m}Tc decay, λ^{Tc} is the ^{99m}Tc decay constant, γ_{Mo} is the branch of ^{99}Tc decay path, I_{Mo} is the emission probability of 140.51 keV gamma of the ^{99}Mo, λ^{Mo} is the ^{99}Mo decay constant, t_e is the decay period elapsed time, and Δt is the counting time interval (900 s).

Term A of Eq. (2) refers to the initial activity of ^{99m}Tc and its contribution to the initial activity of ^{99}Mo. It is impossible to measure this value as it would be necessary to make the activity measurement immediately after the end of irradiation. The initial activity of ^{99m}Tc was determined via the SCALE 6.0 Code (Scale, 2011). The IPEN/MB-01 reactor core was modeled using SCALE 6.0 so that the neutron flux was calculated at the position where the fuel disk was irradiated, and the activity was determined by the ORIGEN-S module. This calculation resulted in 1.268×10^3 Bq initial activity for ^{99m}Tc. The GDS measurements started on average 17 h after irradiation. The activity of ^{99m}Tc after this period of time is 178 Bq and that of ^{99}Mo is nearly 30,000 Bq. Consequently, the initial activity of ^{99m}Tc is negligible compared to that of ^{99}Mo and term A in the Eq. (2) can be neglected.

The absolute values of fission rate in U are obtained from the following relationship:

$$F = \frac{A_{Mo}^0 f_{abs}^{Mo} \cdot F_{rp}}{Y^{Mo}(1 - e^{-\lambda^{Mo} \cdot t_i})}, \quad (3)$$

where f_{abs}^{Mo} is the self-shielding factor of the fuel disk for the gammas of 140.5 keV, I^{NP} is the gamma emission probability for the 140.5 keV gammas from ^{239}Np decay, ε^{Mo} is the detector efficiency for 140.5 keV gammas, λ^{Mo} is the ^{99}Mo decay constant, Y^{Mo} is the effective cumulative fission yield of the ^{99}Mo, t_i is the irradiation period, t_c counting interval and F_{rp} is ramp factor.$\bar{Y}_{Mo}$ the effective cumulative fission yield of ^{99}Mo, is defined by:

$$\bar{Y}_{Mo} = \frac{Y_{Mo}^{25}(\sum_f \Phi)_{25} + Y_{Mo}^{28}(\sum_f \Phi)_{28}}{(\sum_f \Phi)_{25} + (\sum_f \Phi)_{28}}, \quad (4)$$

where $\boldsymbol{Y_{Mo}^i}$ is the cumulative ^{99}Mo fission yield for nuclide i (25 for ^{235}U and 28 for ^{238}U) and $(\Sigma_f \Phi)$ is the fission rate of nuclide i. The effective cumulative fission yield value (Y^{Mo}) of ^{99}Mo was determined employing the ORIGIN 2.0 code (Croff, 1991) that solves the point transmutation equations of the actinides and fission products of the desired fuel and then calculates the inventory activities. The ^{99}Mo effective cumulative fission yield was obtained for a mixture with 95.7% of ^{238}U and 4.3% of ^{235}U.

2.2. Pb collimators

Six different regions of the irradiated fuel disk (Fig. 5) are individually measured employing five lead collimators during the gamma spectrometry. All regions have the same surface area and consequently the same volume. A sixth collimator has the same diameter of the UO_2 disk and is used only to check consistency of the calculated correction factors. The central holes of the collimators were manufactured by the wire EDM (Electrical Discharging Machining) technique. These collimators are inserted in the GDS, one by one, shielding the gammas generated in undesired regions of the UO_2 disk. Thus, relative values of the distribution of the nuclear reaction rates along the radius of the fuel disk can be obtained in a straightforward fashion. During the measurement, the collimators overlap the fuel disk as shown in Fig. 3. The collimators have 1.5 mm height, so the linear gamma attenuations are, respectively, 98.4% and 99.997% for gammas of 140.51 keV and 106.2 keV. Both energies are low enough to minimise the correction factors applied in the measurements. The use of higher energies in the gamma spectrometry would require thicker collimators and consequently higher correction factors.

2.3. Correction factors applied to the experimental results

The use of the collimators on the UO_2 disks changes the GDS geometric efficiency. These effects are corrected using the Geometric Correction Factor (GCF) and the Covered Region Correction Factor (CRCF) that are calculated employing MCNP-5 code (MCNP-5 X-5 Monte Carlo Team, 2003).

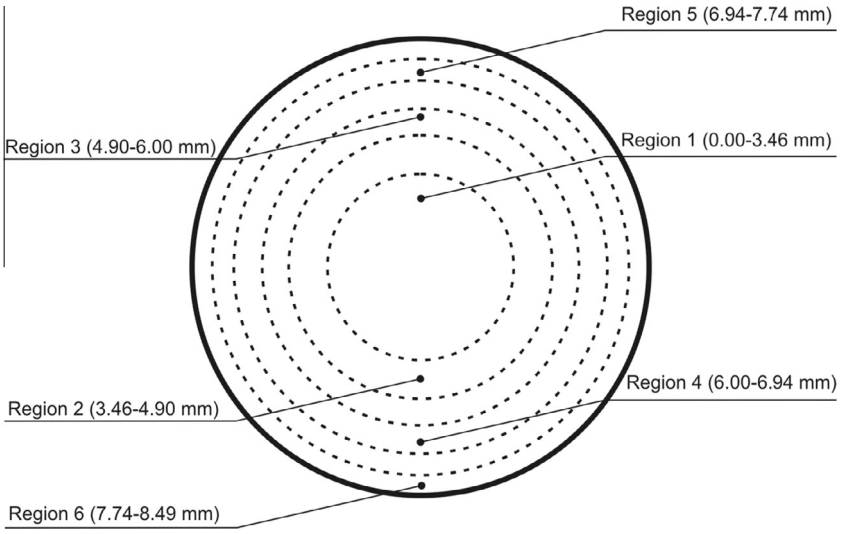

Fig. 5. Six regions of the fuel pellet.

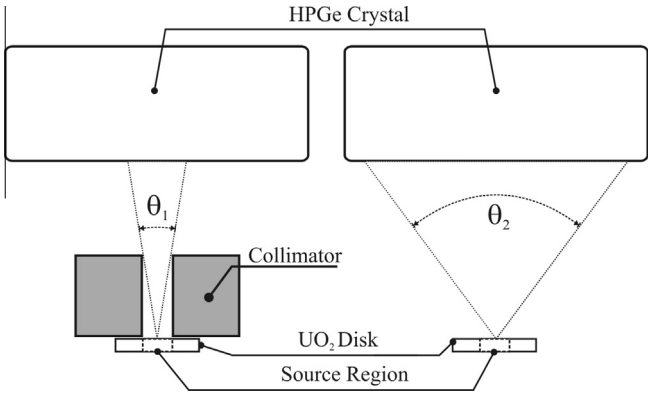

Fig. 6. Illustrative description of the GCF calculation.

2.3.1. The Geometric Correction Factor (GCF)

The GCF factor is the ratio of the detection efficiency with and without the collimator and corrects the solid angle reduction induced by the insertion of the collimator in the GDS. This effect is show in Fig. 6. Pairs of simulations were made to compare the efficiencies with and without the collimators. The ratio between these calculated efficiencies make it possible to obtain this correction factors for each of the six collimators. The efficiencies were determined by modeling individually the GDS with gamma sources of 106.2 keV and 140.5 keV. The Pulse Height Tally (f8) of the MCNP-5 gives the absolute efficiency of the analyzed system. Table 1 shows the values of GCF for the gamma energy 140.5 keV. The results for 106.2 keV are similar.

Table 1 shows that the calculated values of GCF are consistent since they decrease as the source radius increases. The GCF associated uncertainties arise from the Monte Carlo approach adopted in MCNP-5.

The consistency of the calculation of GCF is also checked using collimator number six. The gamma spectrometry measurements were performed with and without this collimator. In this test the A^0_{Mo} value without collimator was 1847.80 ± 31.22 Bq. The A^0_{Mo} value measured with the collimator when multiplied by the GCF for collimator 6 (1.0171) yields 1842.93 ± 35.12 Bq. So, there are very good agreement between the initial activities (measured and corrected measured) giving confidence for the GCF for the other collimators.

2.3.2. Covered Region Correction Factor (CRCF)

The CRCF factor corrects for the undesired contribution of the gammas passing through the covered region of the collimator without interacting with it and hitting the detector, this being more present in the region near the collimator hole. CRCF is calculated in this way to compensate for the non-homogeneity of the reaction rates in the radial direction by correcting for the undesirable detector counting of the each of the covered regions.

To illustrate the determination of CRCF, consider Fig. 7. This figure shows the case for the collimator with the 3.00 mm radius hole. As shown in Fig. 7, the collimator covers three regions that contribute to the detector countings. These are the undesired countings that must be corrected. The factor CRCF is calculated in following way. The gamma source in each of the covered regions was determined from the reaction rates along the pellet radius calculated by MCNP-5. They were normalized to the total reaction rate in the disk. The detector efficiency was calculated by MCPN-5, similarly to the case of GCF, considering the cases with and without collimator. For the example shown in Fig. 7, CRCF is calculated three times; namely for region 6, 5, and 4 respectively. The CRCF in each of these regions is calculated as:

Table 1
GCF for collimators and gamma with 140.5 keV.

Collimator	Source radius (mm)	Efficiency without collimator E_r	Efficiency with collimator EC_r	GCF (ratio E_r/EC_r)
1	1.73	$4.063 \times 10^{-3} \pm 1.1 \times 10^{-5}$	$3.8136 \times 10^{-3} \pm 1.1 \times 10^{-5}$	1.0653 ± 0.0043
2	2.45	$4.059 \times 10^{-3} \pm 1.1 \times 10^{-5}$	$3.9096 \times 10^{-3} \pm 1.1 \times 10^{-5}$	1.0382 ± 0.0041
3	3.00	$4.057 \times 10^{-3} \pm 1.1 \times 10^{-5}$	$3.9502 \times 10^{-3} \pm 1.1 \times 10^{-5}$	1.0270 ± 0.0041
4	3.47	$4.052 \times 10^{-3} \pm 1.1 \times 10^{-5}$	$3.9703 \times 10^{-3} \pm 1.1 \times 10^{-5}$	1.0207 ± 0.0040
5	3.87	$4.052 \times 10^{-3} \pm 1.1 \times 10^{-5}$	$3.9863 \times 10^{-3} \pm 1.1 \times 10^{-5}$	1.0164 ± 0.0040
6	4.245	$4.063 \times 10^{-3} \pm 1.1 \times 10^{-5}$	$3.9948 \times 10^{-3} \pm 1.1 \times 10^{-5}$	1.0171 ± 0.0040

$$CRCF_{j,k} = \frac{Ec_{j,k}C_k}{E_{j,k}}, \tag{5}$$

where *i,j,k* represents, respectively, the gamma energy (i = 1 for capture and i = 2 for fission), the collimator identity and the covered region identity as defined in Fig. 7, $Ec_{j,k}$ is the region k efficiency with the collimator j, $E_{j,k}$ is the region k efficiency without the collimator, C_k is the expected relative reaction rate value in region k calculated by MCNP-5.

The associated uncertainty of CRCF is given by:

$$\sigma_{CRCF_{j,k}} = \sqrt{\left(\frac{C_k\sigma_{Ec_{j,k}}}{E_{j,k}}\right)^2 + \left(\frac{Ec_{j,k}\sigma_{C_k}}{E_{j,k}}\right)^2 + \left(\frac{Ec_{j,k}C_k\sigma_{E_{j,k}}}{E_{j,k}^2}\right)^2}, \tag{6}$$

where $\sigma_{Ec_{j,k}}$ is the uncertainty of the region k efficiency with the collimator j, σ_{C_k} is the uncertainty of the expected relative reaction rate value in region k, and $\sigma_{E_{j,k}}$ is the uncertainty of the region efficiency without the collimator. All uncertainties are statistical uncertainties from MCPN-5.

Table 2 shows the values of CRCF for the gamma energy 140.5 keV. The results for 106.2 keV are similar.

The reaction rates ($T_{i,j}$) for each collimator are defined as:

$$T_{i,j} = GCF_{i,j}\left\{X_0^{i,j} - \left(\sum_{k=j+1}^{6} CRCF_{i,j,k}R_0^i\right)\right\}, \tag{7}$$

where $GCF_{i,j}$ is the geometric correction factor, k represents the covered region of the UO_2 disk, $X_0^{i,j}$ is the corrected counting at the end of the irradiation (C_o) for ^{239}Np or the initial activity (A_o) for the ^{99}Mo, both for collimator j; R_0^i is the corrected counting at the end of the irradiation (C_o) for ^{239}Np or the initial activity (A_o) for the ^{99}Mo without collimator (full disk measurement).

The uncertainty associated with $T_{i,j}$ is given by:

$$\sigma_{T_{y,j}} = \sqrt{\left((X_0^{i,j} - \sum_{k=j+1}^{j} CRCF_{i,j,k}R_0^i)\sigma_{GCF_{i,j}}\right)^2 + \left(GCF_{i,j}\sigma_{X_0^{i,j}}\right)^2 + \left(GCF_{i,j}R_0^i\sigma_{\sum_{k=j+1}^{6} CRCF_{i,j,k}}\right)^2 + \left(GCF_{i,j}\sum_{k=j+1}^{j} CRCF_{i,j,k}\sigma_{R_0^i}\right)^2}, \tag{8}$$

where $\sigma_{GCF_{i,j}}$ is the uncertainty of $GCF_{i,j}$, $\sigma_{X_0^{i,j}}$ is the uncertainty of the corrected counting at the end of the irradiation (C_o) for ^{239}Np or the initial activity (A_o) for the ^{99}Mo with collimator j,

$$\sigma_{\sum_{k=j+1}^{6} CRCF_{i,j,k}} = \sqrt{\sum_{k=j}^{6}\left\{\left(\frac{C_k\sigma_{Ec_{j,k}}}{E_{j,k}}\right)^2 + \left(\frac{Ec_{j,k}\sigma_{C_k}}{E_{j,k}}\right)^2 + \left(\frac{Ec_{j,k}C_k\sigma_{E_{j,k}}}{(E_{j,k})^2}\right)^2\right\}}, \tag{9}$$

$\sigma_{R_0^i}$ is the uncertainty of the corrected counting at the end of the irradiation (C_o) for ^{239}Np or the initial activity (A_o) for the ^{99}Mo without collimator (full disk measurement).

The sum of the contribution of each of the covered regions is subtracted from the total reaction rate as show in Eq. (7).

2.4. The relative reaction rates

The relative reaction rates inside of the fuel pellets are defined as:

$$A_{i,j} = \frac{T_{i,j} - T_{i,(j-1)}}{R_0^i}, \tag{10}$$

with $T_{i,6} = R_0^i$ and $T_{i,0} = 0.0$.

The uncertainty associated with $A_{i,j}$ is given by:

$$\sigma_{A_{i,j}} = \sqrt{\left(\frac{\sigma_{T_{i,j}}}{R_0^i}\right)^2 + \left(\frac{\sigma_{T_{i,(j-1)}}}{R_0^i}\right)^2 + \left(\frac{(T_{i,j} - T_{i,(j-1)})\sigma_{R_0^i}}{(R_0^i)^2}\right)^2 - \frac{2\sigma_{T_{i,j}}\sigma_{T_{i,(j-1)}}}{(R_0^i)^2}Cov(T_{i,j}, T_{i,(j-1)})} \tag{11}$$

It is important to say that in the determination of the relative reaction rates there is no need to use the self-shielding factor of the fuel disk, the gamma emission probability and the ramp factor since these are constants for all measurements.

The covariance ($Cov(T_{i,j},T_{i,j-1})$) presented in Eq. (11) was calculated employing the MCNP-5 code. The methodology is similar to the one presented in Section 4 since it is a reaction rate calculation of two disk regions. For example, the covariance in region 6 ($Cov(T_{i,6},T_{i,5})$) was determined by calculating the reaction rates for full disk and for the sum of the regions 1,2,3,4 and 5 as:

$$Cov(T_{i,6}, T_{i,5}) = \frac{(\sigma_{T_{i,5}})^2 + (\sigma_{T_{i,6}})^2 - (\sigma_{A_{i,6}})^2}{2\sigma_{T_{i,5}}\sigma_{A_{i,6}}} \tag{12}$$

The covariance involving other regions was determined in a similar fashion. Tables 3 and 4 show the final results.

3. The experimental results

Before going into the presentation of the total fission and radiative capture in ^{238}U reaction rate values along the pellet radius, consider a consistency check for the experimental methodology presented in this paper. Table 5 presents the measured reaction rates employing the new technique using the ^{99}Mo as a fission tracker and the 106.2 keV photopeak gamma emission of ^{239}Np for the radiative capture in ^{238}U. Table 6 compares the spectral index C8/F (without cadmium sleeve) obtained in this work to that accepted by IRPhE (dos Santos et al., 2012) as an international benchmark.

Table 6 shows that the value of the spectral index C8/F obtained using the experimental methodology developed in this paper is consistent with the benchmark reference value, thus validating the results of nuclear reaction rates presented here. The measured result of C8/F employing the proposed approach of this paper falls inside of the $1-\sigma$ interval of the experimental uncertainties of both approaches. The uncertainty related to C8/F of this work is approximately 6.2% and is due mainly to the uncertainty of the GDS efficiency.

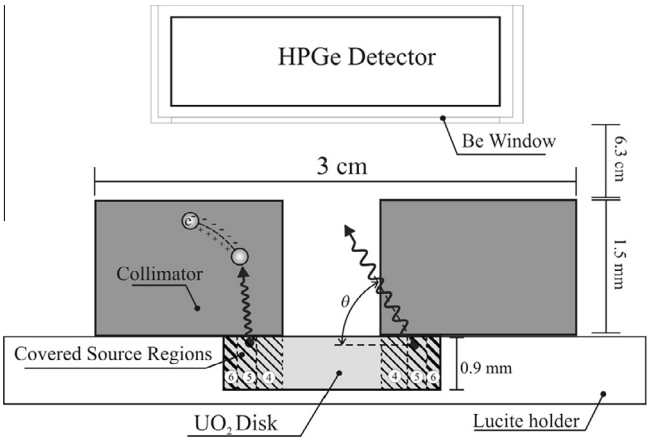

Fig. 7. Illustrative description of the CRCF calculation.

Table 2
CRCF for each covered region for collimators (j) and gamma with 140.5 keV.

Collimator hole radius (mm)	Region (k)	$CRCF_{2,j,k}$
1.73	2	$8.101 \times 10^{-2} \pm 4.1 \times 10^{-4}$
	3	$2.670 \times 10^{-2} \pm 2.3 \times 10^{-4}$
	4	$2.670 \times 10^{-2} \pm 2.3 \times 10^{-4}$
	5	$2.660 \times 10^{-2} \pm 2.3 \times 10^{-4}$
	6	$2.671 \times 10^{-2} \pm 2.3 \times 10^{-4}$
2.45	3	$1.1298 \times 10^{-1} \pm 4.9 \times 10^{-4}$
	4	$2.673 \times 10^{-2} \pm 2.3 \times 10^{-4}$
	5	$2.656 \times 10^{-2} \pm 2.3 \times 10^{-4}$
	6	$2.671 \times 10^{-2} \pm 2.3 \times 10^{-4}$
3.00	4	$1.3944 \times 10^{-1} \pm 5.5 \times 10^{-4}$
	5	$2.695 \times 10^{-2} \pm 2.3 \times 10^{-4}$
	6	$2.672 \times 10^{-2} \pm 2.2 \times 10^{-4}$
3.47	5	$1.6971 \times 10^{-1} \pm 6.2 \times 10^{-4}$
	6	$2.7970 \times 10^{-2} \pm 2.3 \times 10^{-4}$
3.87	6	$1.8479 \times 10^{-1} \pm 6.4 \times 10^{-4}$

Table 3
$Cov(T_{1,j},T_{1,(j-1)})$: covariance for the relative reaction rate for ^{238}U radiative capture.

j	Bare	Epicadmium
2	0.820255	0.8578856
3	0.932508	0.9086335
4	0.944263	0.9374450
5	0.946245	0.9521165
6	0.820802	0.8292472

Table 4
$Cov(T_{2,j},T_{2,(j-1)})$: Covariance table for relative reaction rate values for total fissions.

j	Bare	Epicadmium
2	0.9172006	0.9036742
3	0.9561902	0.9450826
4	0.9622277	0.9778292
5	0.9922938	0.9843522
6	0.9837796	0.9800097

The irradiations to determine the reaction rates along the radial direction of the fuel pellets were performed in a dual mode. Two for the bare UO_2 disk and two for the Cadmium covered case. These repetitions reduce the statistical uncertainty and also serve as the experiment reproducibility guarantee. The reproducibility was within the experimental uncertainties. The moderator temperature was kept between 19.5 °C and 21 °C in all irradiations. This was achieved employing the heating/cooling system of the facility. Twelve thermocouples distributed evenly along the core as in (dos Santos et al., 2004) were utilized to cope with this task.

Table 5
Full disk reaction rate values for fission and radiative capture in ^{238}U.

Nuclear reaction rate type	Value (reactions/s)
^{238}U Radiative Capture (C8)	$4.78 \times 10^6 \pm 2.1 \times 10^5$
Fission	$1.562 \times 10^7 \pm 7.0 \times 10^5$

Table 6
C8/F spectral index values without cadmium sleeve.

	C8/F
IRPhE Benchmark	0.312 ± 0.003
Experimental data from Molybdenum Analysis	0.306 ± 0.019

Table 7
Relative reaction rate values for ^{238}U radiative capture reaction rates.

Disk region	Bare	Epicadmium	Subcadmium
1	0.1238 ± 0.0014	0.1262 ± 0.0012	0.115 ± 0.035
2	0.1372 ± 0.0029	0.1313 ± 0.0026	0.157 ± 0.042
3	0.1454 ± 0.0041	0.1388 ± 0.0033	0.168 ± 0.046
4	0.1554 ± 0.0054	0.1493 ± 0.0044	0.176 ± 0.052
5	0.1730 ± 0.0067	0.1692 ± 0.0077	0.186 ± 0.062
6	0.2652 ± 0.0052	0.2851 ± 0.0068	0.197 ± 0.079

Table 8
Relative total fission reaction rate values.

Disk region	Total	Epicadmium
1	0.1435 ± 0.0044	0.1509 ± 0.0071
2	0.1589 ± 0.0066	0.1542 ± 0.0095
3	0.1654 ± 0.0076	0.1661 ± 0.0100
4	0.1757 ± 0.0082	0.1663 ± 0.0116
5	0.1825 ± 0.0093	0.1967 ± 0.0166
6	0.1740 ± 0.0115	0.1657 ± 0.0187

Table 7 shows the average relative ^{238}U radiative capture reaction rate values. The experimental data are shown for the bare, epicadmium and subcadmium spectral energy ranges. These results were obtained using Eqs. (10) and (11) and were normalized to the full disk measurement. The subcadmium values are obtained indirectly by simply subtracting the bare and the epicadmium results.

Similarly, Table 8 shows the experimental total fission reaction rates in relative units for bare and epicadmium cases. The results for the subcadmium region were not possible to obtain because of the yield dependence. There is no data available for the ^{99}Mo fission product yield in the epicadmium energies spectrum.

Tables 7 and 8 show clearly the spatial self-shielding effects occurring in the ^{238}U(n,γ) and in the total fission reaction rates. The self-shielding effect is more pronounced in the neutron capture rates in ^{238}U being a little bit more severe for the epicadmium events. Table 7 also shows that approximately 26% of captures in ^{238}U(n,γ) reactions occur in the outermost region of the fuel pellets. The self-shielding effect for the total fissions is less pronounced but the experimental results reveal a very surprising effect. The total fission reaction rate shows its maximum value in region 5; not in the outermost region. This surprising result has never being observed in any of the previous works related to the spatial measurements of the reaction rates inside of the fuel pellet.

4. Theoretical analysis and results

The theoretical analyses applied to the reaction rate experiments were carried out in a stochastic approach employing MCNP-5, together with ENDF/B-VII.0 (Oblozinsky and Herman, 2006) as the basic nuclear data library. The geometric model (both axial and radial) and the material and geometric data applied in the theoretical analysis arose from LEU.COMP.THERM.077 (dos Santos et al., 2004) which is a full 3-D core modeling of the IPEN/MB-01 reactor. However the set of measurements shown here had no baffle plates. The cadmium insertion apparatus and its sleeve were modeled explicitly taking into consideration the critical control bank position BC1 and BC2 changes. Fig. 8 shows in a schematic way the sampling model and the ^{238}U capture and fission reaction rates tally regions. Since the ^{238}U disk is in the asymptotic region of the IPEN/MB-01 core, the axial tally height was increased to 1.0 cm in order to improve the Monte Carlo statistics.

The KCODE option was used to calculate reaction rates and simulate the irradiation of the target over several fission cycles. The tally F4 was used for the calculation of the reaction rates. Six tallies were created to represent the regions measured within the collimators. The results are the reaction rates of a given type occurring in a cell in relative units.

Uncertainties associated with the reaction rate values were minimized by running 6.4×10^9 histories being less than 1% and 0.5%, respectively, for the cases with and without cadmium sleeve.

The calculated results for the normalized ^{238}U(n,γ) and total fissions from the theoretical approach based on the MCNP-5 code using the ENDF/B-VII.0 library are shown respectively in Tables 9 and 10. The results are shown for the irradiated UO_2 disk with and without cadmium sleeve using the same tally in both simulations and normalized in function of the full disk reaction rate estimate (without collimator). The subcadmium reaction rates are shown only for the ^{238}U(n,γ) reaction rates and were determined by subtracting the corresponding results from both simulations and renormalizing accordingly.

5. Theory/experiment comparisons

The relationship (C-E)/E is frequently used to perform a quantitative comparison between the calculation values and those obtained via experiments. Here C is the calculated value from MCNP-5 and E is the experimental value of the reaction rates. This is the most appropriate way to compare calculation and experiment. Comparing the uncertainty of (C-E)/E with (C-E)/E itself it is possible to check if the discrepancies between calculation and experiment fall inside of 1 – σ standard deviation of the experimental uncertainty. Table 11 shows this quantity for the ^{238}U radiative capture values as a function of the pellet region.

With the exception of region 1, Table 11 shows that the calculated relative values for the total ^{238}U(n,γ) capture rates are in excellent agreement to the experimental values. Their (C-E)/E values fall inside of the 1 – σ standard deviation of the experimental uncertainty for all other radial regions of the fuel disk. The (C-E)/E value for region 1 shows a discrepancy of 9% and it is well outside of the1 – σ standard deviation. The reason for this discrepancy which will be discussed shortly can be credited to the thermal fission cross section of ^{235}U. Still in the same table, the (C-E)/E values for the epicadmium capture reaction rates of ^{238}U show excellent

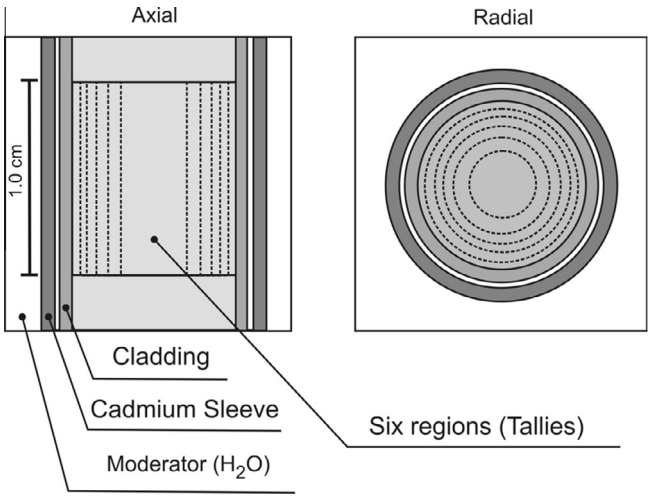

Fig. 8. Details of the axial and radial modeling of the sampling regions.

Table 9
Calculated values for radiative capture reaction rates in ^{238}U (in relative unities).

Disk region	Total	Epicadmium	Subcadmium
1	0.13496 ± 0.00084	0.1248 ± 0.0014	0.146 ± 0.002
2	0.13849 ± 0.00074	0.1324 ± 0.0015	0.145 ± 0.002
3	0.14437 ± 0.00076	0.1385 ± 0.0015	0.151 ± 0.002
4	0.15242 ± 0.00081	0.1482 ± 0.0016	0.157 ± 0.002
5	0.16825 ± 0.00095	0.1658 ± 0.0018	0.171 ± 0.002
6	0.2615 ± 0.0024	0.2902 ± 0.0036	0.230 ± 0.005

Table 10
Calculated values for the total fission reaction rates (in relative unities).

Disk region	Total	Epicadmium
1	0.15732 ± 0.00049	0.1650 ± 0.0015
2	0.16003 ± 0.00042	0.1656 ± 0.0015
3	0.16386 ± 0.00041	0.1664 ± 0.0015
4	0.16795 ± 0.00040	0.1667 ± 0.0015
5	0.17270 ± 0.00042	0.1677 ± 0.0015
6	0.17814 ± 0.00045	0.1686 ± 0.0015

Table 11
(C-E)/E values for the radiative capture reaction rates in ^{238}U.

Disk region	Total (%)	Epicadmium (%)	Subcadmium (%)
1	9.0 ± 1.4	−1.1 ± 1.5	27.2 ± 3.4
2	1.0 ± 1.3	0.8 ± 1.8	−8.8 ± 1.6
3	−0.7 ± 1.0	−0.2 ± 1.3	−11.7 ± 1.8
4	−1.9 ± 1.2	−0.7 ± 1.6	−11.9 ± 3.0
5	−2.7 ± 1.2	−2.0 ± 2.4	−8.4 ± 3.0
6	−1.4 ± 1.9	1.8 ± 2.5	20.8 ± 3.0

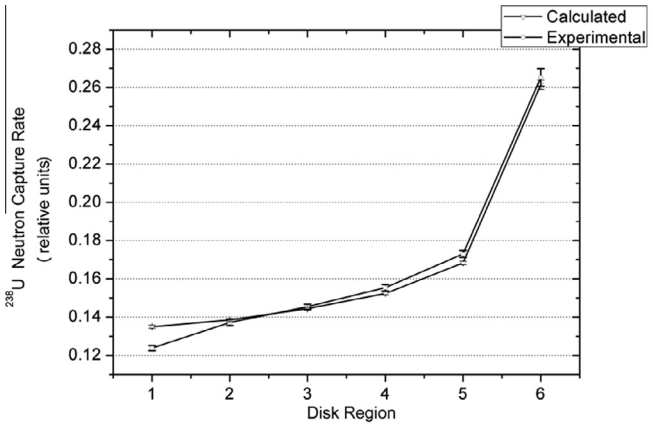

Fig. 9. Comparison between calculated and experimental values for ^{238}U radiative capture in the six regions.

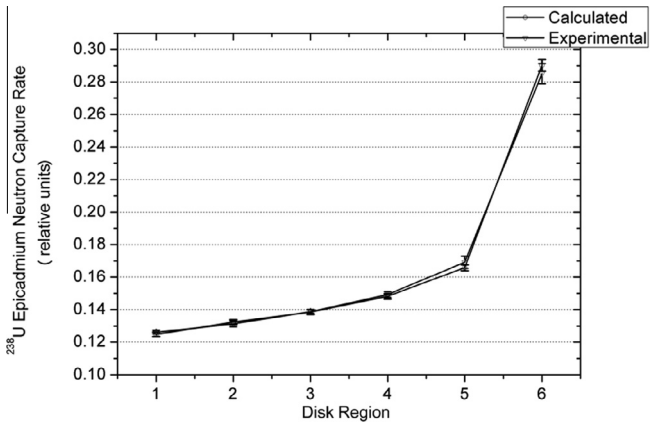

Fig. 10. Comparison between calculated and experimental values for ^{238}U epicadmium radiative capture in the six regions.

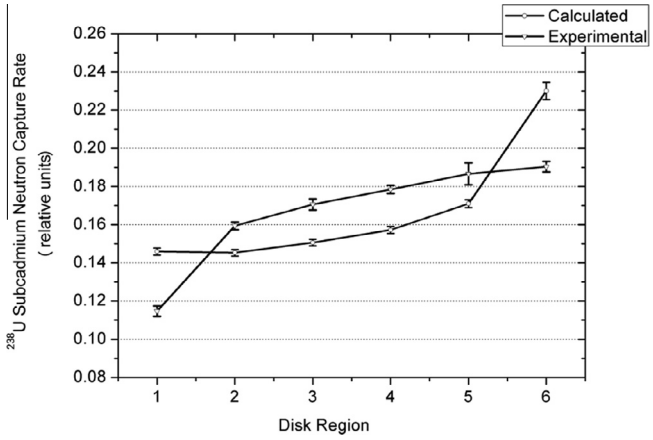

Fig. 11. Comparison between calculated and experimental values for ^{238}U subcadmium radiative capture in the six regions.

results with all their values inside of the 1 – σ standard deviation of the experimental uncertainty. These comparisons show that the neutron capture cross sections in the resolved resonance region of ^{238}U are well represented in the ENDF/B-VII.0 library. The long term overprediction of the ^{238}U neutron epithermal capture (Courcelle, 2006) appears to be eliminated with the improvements in the recent nuclear data libraries. The experiments performed at the IPEN/MB-01 reactor support the changes in the ^{238}U nuclear data incorporated in ENDF/B-VII.0. This comparison reinforces the fact that the reason for the discrepancies found in the region 1 for the ^{238}U capture rates for the bare case reside in the thermal region.

Figs. 9 and 10 show the comparison of the relative reaction rates in a graphical form for the bare and cadmium covered cases, respectively.

Fig. 11 and Table 11 show the comparison between calculated and experimental values for the ^{238}U(n,γ) reaction rates in the subcadmium neutron energy region. Contrary to the case of the epithermal region, here the comparison between theory and experiment show discrepancies both in the shape; i.e., the radial dependence, as well as in the magnitude of the (C-E)/E values. All discrepancies are outside of the 1 – σ standard deviation of the experimental uncertainty which evidences some deficiencies in the thermal cross sections of ENDF/B-VII.0. The IPEN/MB-01 reactor is an experimental facility in which the majority of the reaction rate events occur in the thermal energy region. In this context, ^{235}U

Table 12
C-E/E reaction rate values for the total fission.

Disk region	Total (%)	Epicadmium (%)
1	9.7 ± 3.4	9.3 ± 5.3
2	0.7 ± 1.6	7.4 ± 2.7
3	−1.0 ± 1.4	0.2 ± 2.2
4	−4.4 ± 1.3	0.2 ± 2.1
5	−5.4 ± 1.2	−14.7 ± 3.2
6	2.4 ± 1.7	1.7 ± 3.3

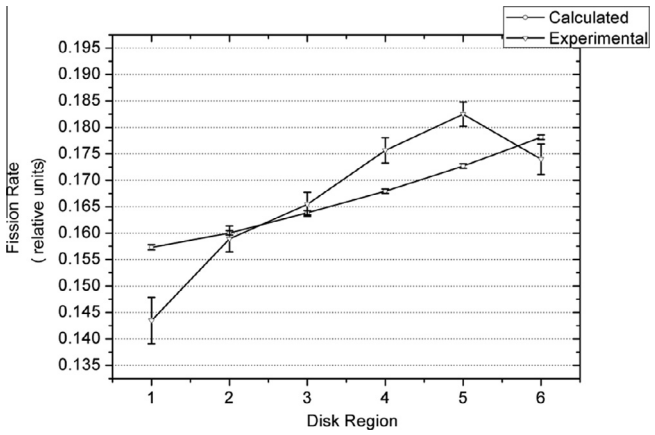

Fig. 12. Comparison between calculated and experimental values for the total fissions.

plays an important role since around 86% of the fissions in this nuclide occur in the thermal neutron energy region. Moreover, around 70% of the total neutron absorptions in the thermal neutron energy range are due to ^{235}U. Consequently, the thermal ^{235}U cross sections play an important role in the spatial and energetic neutron flux in this neutron energy region of the IPEN/MB-01 core. Therefore, the source of the discrepancies in the thermal neutron captures in ^{238}U may be credited mostly to the ^{235}U thermal data. This statement will become clearer in the coming paragraphs.

Table 12 shows the (C-E)/E values for the total fission values for all regions. ^{235}U is responsible for more than 97% of the total fissions and most of that (nearly 86%) occur in the thermal region. Therefore the comparison between theory and experiment is basically a comparison of thermal events. Similarly to the case of the subcadmium ^{238}U neutron captures, the relative total fission reaction rates (C-E)/E values show severe discrepancies. Table 12 reveals that for the bare case the (C-E)/E values are inside of the 1 – σ standard deviation only for regions 2 and 3. The remaining regions show discrepancies that are well outside of the 1 – σ standard deviation of the experimental uncertainty. The comparison between theory and experiment for this case is better represented in a graphical form as shown in Fig. 12.

Fig. 12 shows clearly that the disagreement of the relative total fission rates is not only in magnitude but also in the radial shape of the comparison. The fission rate peak in region 5 is not foreseen by the theoretical predictions. The probable reason for the thermal reaction rate discrepancies is the ^{235}U nuclear data in this region. The ^{235}U cross sections in the thermal region are controlled mainly for the resonance located at 0.3 eV. Below this point the cross sections exhibit a shape close to 1/v. Fig. 13 shows the thermal spectra in the fuel region and the ^{235}U fission cross section. The thermal spectra were calculated by HAMMER-TECHNION [Barhen et al., 1978]. The calculated thermal spectra resemble a Maxwellian distribution which is the expected behavior for the neutron spectra at this energy range of a thermal facility. The ^{235}U fission reaction rate

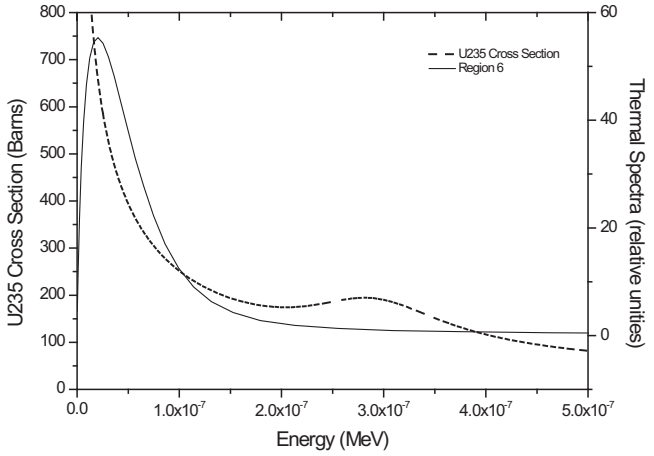

Fig. 13. Thermal Spectra and the ^{235}U fission cross sections in the thermal region.

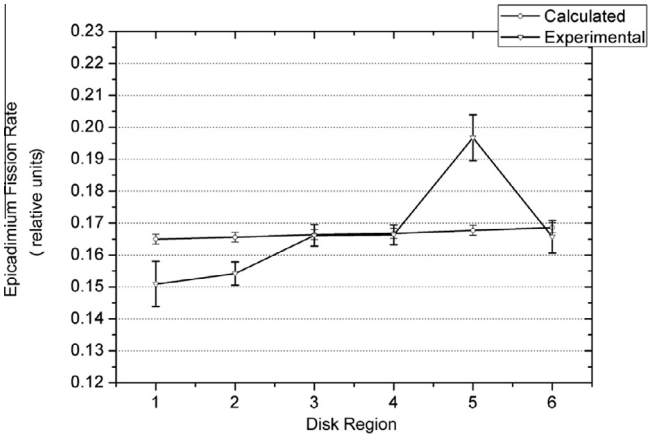

Fig. 14. Comparison between calculated and experimental values for epicadmium fission in the six regions.

at the thermal region is a convolution between the ^{235}U fission cross section and the neutron spectra. As the radial position in the fuel pellet goes into the central region, the thermal neutron spectra becomes harder and harder and its thermal peak moves slightly to the region of higher energies but still inside of the thermal neutron energy region. Since the experimental work shows an increase of the ^{235}U fission rate for the disk region 5, it might suggest that the ^{235}U fission cross section may not have the shape as presented in the nuclear library ENDF/B-VII.0. Weigmann et al. (1990) already suggested that the 1/v ^{235}U cross section shape presented in several nuclear data libraries is not a good representation of this quantity in the thermal neutron energy range thus somewhat supporting to the validity of the experimental work of this paper.

The comparison between calculated and experimental values for epicadmium total fission reaction rates is also shown in Table 12. Fig. 14 shows the comparison for epicadmium fission rates in a graphical form. Here, the agreement between theory and experiment is better than that of the thermal region, although there is a severe disagreement is region 5. Cadmium is a very good thermal neutron absorber. Even so, the MCNP-5 analyses show that the epithermal fissions are still contaminated by a small portion of thermal fission. Around 1% of the thermal neutron flux penetrates through the cadmium sleeve and induces fissions. This 1% of thermal fission contribution means about 10% of the epithermal fission rates in the several regions analyzed in this paper. Consequently, the thermal fissions contamination in the epithermal fission rate can be a good reason for the discrepancy found between theory and experiment in region 5.

6. Conclusions

The proposed experimental method for the determination of the reaction rates in the radial direction of the fuel pellets was successfully performed and it was demonstrated to be feasible and appropriate. The experiments with and without cadmium sleeve in the core of the IPEN/MB-01 reactor were successfully performed and produced data of good quality.

It has been shown that it is possible to use ^{99}Mo and ^{99m}Tc to infer the fission rate. It was found that the ^{99}Mo is ideal for such measurements because of its linear formation as a function of the irradiation period and the low energy of the emitted gammas resulting in small correction factors.

The theory/experiment comparisons in the sampled regions reveal that the agreement of the MCNP-5 results together with the ENDF/B-VII.0 library to the experimental values is very good for both total and ^{238}U epicadmium radiative capture. However the same can not be said for the thermal region. Subcadmium measurements of ^{238}U radiative capture show higher discrepancies and the main reason may be credited to the ^{235}U thermal neutron cross sections which might not be well represented in the ENDF/B-VII.0 nuclear data library.

The relative deviation between calculated and experimental values for the fission rate shows discrepancies that are beyond of the error bars considering the range of 1σ of the experimental uncertainty in regions 1 and 5 for measurements for the case without cadmium sleeve. For both experimental measurements region 5 shows an increase in the ^{235}U fission rate which is not foreseen by the theoretical model. This might indicate that the ^{235}U fission cross sections are not well represented in the thermal energy region.

Acknowledgments

The authors are grateful to Comissão Nacional de Energia Nuclear (CNEN) for providing the financial supports of a doctor scholarship for Luís Felipe Liambos Mura. The authors would also like to thank the operational staff of the IPEN/MB-01 reactor for their patience and efficient operation during the course of the experiment.

References

Andrianov, A.N. et al., 2008. Simulation of neutron-physical processes in the surface layer of a fuel kernel. At. Energ. 104 (6), 463–469.
Barhen, J., Rothenstein, W., Taviv, E., 1978. The Hammer Code System, NP-565. Technion-Israel Institute of Technology, Haifa, Israel.
Briesmeister, J.F. (Ed.), 2000. MCNP – A General Monte Carlo N-Particle Transport Code, Version 4C. Los Alamos National Laboratory Report, LA. 13709-M..
Briggs, J.B. (Ed.), 2012. International Handbook of Evaluated Criticality Safety Benchmark Experiments NEA/NSC/DOC(95)03/I. Nuclear Energy Agency, Paris. September 2012 Edition.
Charlton, W.S., Parish, T.A., Raman, S., Shinohara, N., Andoh, M., 1996. "Delayed Neutron Emission Measurements From Fast Fission of U-235 and Np-237", PHYSOR 1996. Mito, Japan.
Courcelle, A. et al., 2006. Nuclear Data for Improved LEU-LWR Reactivity Predictions. OECD Nuclear Energy Agency. NEA/WPEC-22.
Croff, A.G., 1991. Origen2: A Revised and Updated Version of the Origen Computer Code. Oak Ridge National Laboratory.
De Kruijf, W.J.M., 1993. ROLAIDS-CPM: A Code for Accurate Resonance Absorption Calculations. ECN (Energy research Centre of the Netherlands), Netherlands.
Dos Santos, A., et al., 2004. LEU-COMP-THERM-077: critical loading configurations of the IPEN/MB-01 reactor. In: Briggs J. Blair (Ed.). International Handbook of Evaluated Criticality Safety Benchmark Experiments, NEA/NSC/DOC (95)03/I, Paris, September.

Dos Santos, A. et al., 2005. The inversion point of the isothermal reactivity coefficient of the IPEN/MB-01 reactor—II: theoretical analysis. Nucl. Sci. Eng. 151, 237–250.

Dos Santos, A. et al., 2012. IPEN (MB01)-LWR-COEF-KIN-RESR-001: Reactor Physics experiments in the IPEN/MB-01 Research Reactor Facility. International Handbook of Evaluated Reactor Physics Benchmark Experiments. NEA/NSC, pp. 1–142.

Eckhardt, R., 1987. Stan Ulam, John von Neumann, and the Monte Carlo method (PDF). Los Alamos Science, Special Issue 15, 131–137.

Edenius, Kim Ekberg, Bengt H. Forssén, Dave Knott, 1995. CASMO-4, A Fuel Assembly Burnup Program, User's Manual. STUDSVIK/SOA-95/1, Studsvik of America Inc.

Goltsev, A.O., Davidenko, V.D., Tsibulsky, V.F., Lekomtsev, A.A., 2003. The influence of a non-uniform radial temperature distribution in the fuel on the results of calculation of transients. Ann. Nucl. Energy 30, 1135–1153.

Gray, P.W., Ahmad, A., 1985. Linear classes of Ge(Li) detector efficiency functions. Nucl. Instrum. Methods Phys. Res. A237, 577–589.

Hellstrand, E., 1996. Measurement of resonance integrals reactor physics in the resonance and thermal range. In: Proc. of the National Meeting of the American Nuclear Society, San Diego.

Hwang, R.N., Wigner, E.P., 2004. An overview of resonance theory in reactor applications. In: Reactor Physics. Argonne National Laboratory, pp. 96–101. ANL/NE/CP-113868.

Macku, K., Jatuff, F., Murphy, M.F., Joneja, O.P., Bischofberger, C.R., Chawla, R., 2006. Advanced foil activation techniques for the measurement of within-pin distributions of the $^{63}Cu(n.g)^{64}Cu$ reaction rate in nuclear fuel. Nucl. Instrum. Methods Phys. Res., 393–400

Macku, K., Jatuff, F., Murphy, M., Plaschy, M., 2007. Radial and azimuthal ^{235}U fission and ^{238}U capture distributions in BWR UO2 pins: CASMO-4 and MCNP-4C versus activation foil measurements. Nucl. Sci. Eng. 155, 96–101.

Matsumoto, H., Ouisloumen, M., Takeda, T., 2005. Development of spatially dependent resonance shielding method. J. Nucl. Sci. Technol. 8, 688–694.

Matzke, H., 1992. On the rim effect in high burnup UO2 LWR fuels. J. Nucl. Mater. 189, 141–148.

MCNP-5 X-5 Monte Carlo Team, 2003. MCNP – A General Monte Carlo N-Particle Transport Code. Version 5. LA-UR-03-1987, April.

Nakajima, K., Akai, M.A.S.T., 1994. Measurement of the modified conversion ratio by gamma-ray spectrometry of fuel rods for water-moderated UO2 cores. Nucl. Sci. Eng. 116, 138–146.

Nakajima, K., Akai, M.A.S.T., 1995. Modified conversion ratio measurement in light water- moderated UO2 lattices. Nucl. Technol. 113, 375–379.

Nakajima, K., Akai, M.A.S.T., Yamamoto, T., Suzaki, T., 1994. Measurement and analyses of the ratio of ^{238}U captures to ^{235}U fission in low-enriched UO2 tight lattices. J. Nucl. Sci. Technol. 31, 1160–1170.

Oblozinsky, O., Herman, M., 2006. Special Issue on Evaluated Nuclear Data File ENDF/B-VII.0. Nuclear Data Sheets. 107. No. 12.

Sanchez, R., Bounds, J., Bredeweg, T., Goda, J., Grove, T., Hayes, D., Jackman, K., Mckenzie, G., Myers, W., 2014, Reaction Rate, Fission Product Yield, and Rossi-Alpha Measurements Using a HEU Metal, Copper Reflected Critical Assembly, Physor 2014, Kyoto, Japan.

SCALE: A Comprehensive Modeling and Simulation Suite for Nuclear Safety Analysis and Design, ORNL/TM-2005/39, Version 6.1, June 2011. Available from Radiation Safety Information Computational Center at OakRidge National Laboratory as CCC-785.

Stoker, C.C., Weiss, Z.J., 1996. Spatially dependent resonance cross-sections in a fuel rod. Ann. Nucl. Energy 23, 765–778.

Weigmann, H., Keck, B., Wartena, J.A., Geltenbort, P., Schreckenbach, K., 1990. Measurement of η of ^{235}U for subthermal neutron energies, 1990. International Conference in Physics of Reactors: Operation. Design and Computation. Marseille. April, vol. 2326.

Williams, T., Chawla, R., Grimm, P., Joneja, O.P., Seiler, R., Ziver, A., 1998. New experiments at a zero-power facility using power reactor fuel, Proceedings of the international Conference on Physics of Nuclear Science and Technology, Long Island, October, pp. 720–727.